Revised Monday, December 22, 2014

Simulations of the Tropical General Circulation with a Multiscale Global Model

David Randall, Charlotte DeMott, Cristiana Stan, Marat Khairoutdinov,

James Benedict, Rachel McCrary, Katherine Thayer-Calder, and Mark Branson

Prepared for the *Yanai Memorial Volume*

Abstract

Cloud processes play a central role in the dynamics of the tropical atmosphere, but for many years the shortcomings of cloud parameterizations have limited our ability to simulate and understand important tropical weather systems such as the Madden-Julian Oscillation. Since about 2001, "super-parameterization" has emerged as a new path forward, complementing but not replacing studies based on conventional parameterizations. This chapter provides an overview of work with super-parameterization, including a discussion of the method itself, and a summary of key results.

Introduction

The tropics strongly absorb solar radiation at all times of year. Much of that solar energy is used to evaporate water at the Earth's surface. The water vapor thus added to the tropical atmosphere can be lofted to form beautiful convective cloud systems, which are organized on scales ranging from a few kilometers to many thousands of kilometers. The resulting weather systems include squall lines, tropical cyclones, and continent-spanning monsoons. The intense, cloudy convective updrafts occupy only a tiny fraction of the tropics, but they carry prodigious amounts of energy upward through the depth of the troposphere. The outflows from the tops of the convective towers feed divergent upper-tropospheric winds, which carry energy poleward, and so contribute to the Earth's global energy balance. This cloud-filled, multiscale tropical circulation was the main subject of Michio Yanai's research.

In atmospheric global circulation models (GCMs), the small-scale processes at work in convective cloud systems must be included through simplified sub-models called

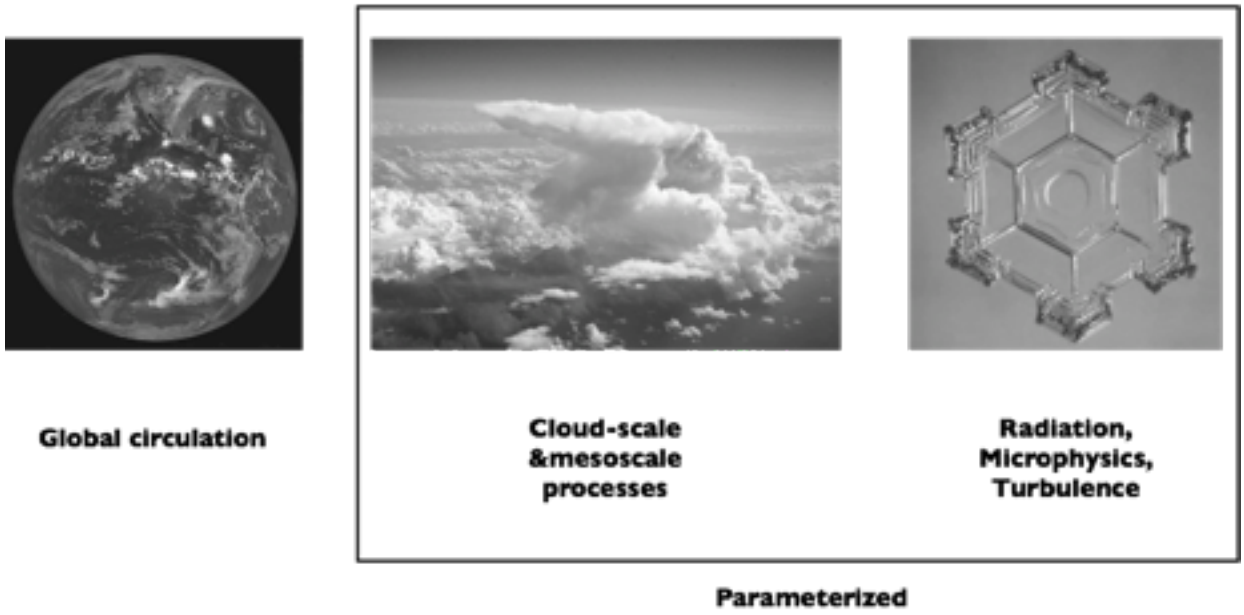

Fig. 1: In conventional GCMs, the global circulation is explicitly simulated. Parameterized processes include cloud-scale and mesoscale dynamics, and also radiative transfer, microphysics, and turbulence.

parameterizations (Fig. 1). Cloud parameterizations have been under development since the 1960s. A lot of progress has been achieved, but major difficulties remain (Randall et al., 2003 a).

In 1999, NCAR[1] scientists Wojciech Grabowski and Piotr Smolarkiewicz created a "multiscale" GCM in which the physical processes associated with clouds were represented by implementing a simple "cloud-resolving" model (CRM) within each grid column of a low-resolution global model (Grabowski and Smolarkiewicz, 1999; Grabowski, 2001, 2004). In this approach, parameterizations of radiation, cloud microphysics, and turbulence (including small

[1] NCAR is the National Center for Atmospheric Research.

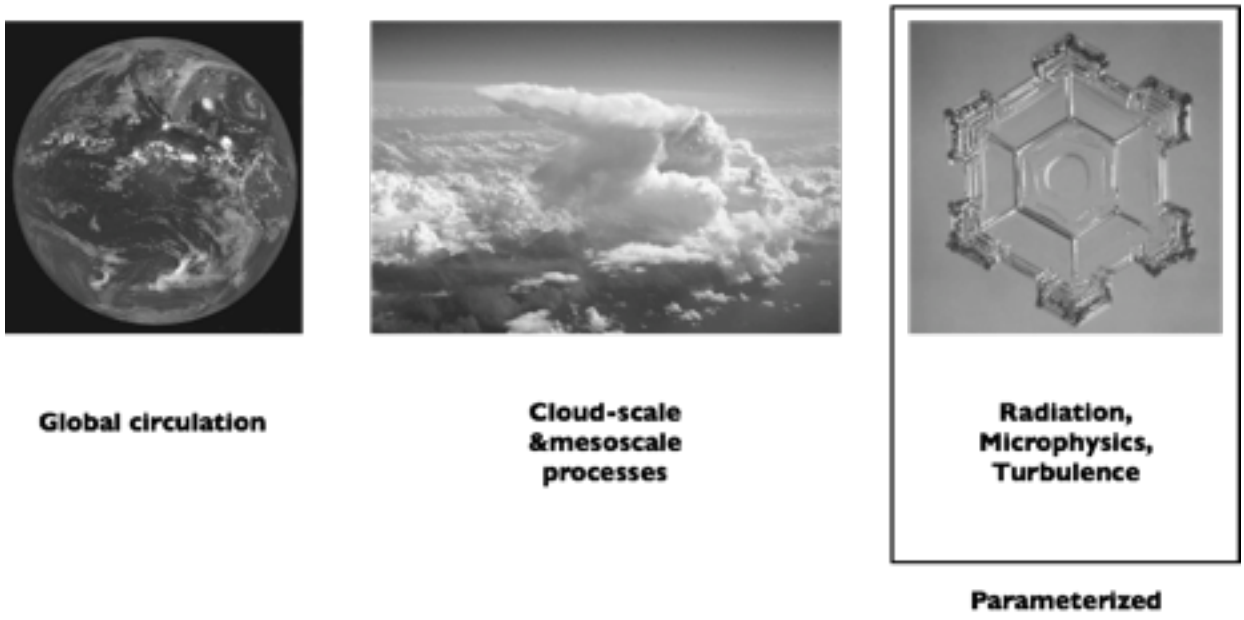

Fig. 2: When a CRM is used as a super-parameterization in a GCM, the cloud and mesoscale dynamics are explicitly simulated, but radiation,microphysics, and turbulence must still be parameterized on the CRM's grid. Compare with Fig. 1.

clouds) are still needed (Fig. 2), but larger clouds and some mesoscale processes are explicitly (though crudely) simulated.

In highly idealized experiments, Grabowski and Smolarkiewicz found that their multiscale model produced promising simulations of organized tropical convection. In particular, the simulations showed propagating convective systems that resembled the Madden-Julian Oscillation[2] (MJO; Madden and Julian, 1971, 1972). The MJO is an eastward-propagating tropical disturbance that spans thousands of kilometers in the zonal direction, with an irregular period in the range 40-50 days. Despite its large spatial and temporal scales, and its powerful effects on tropical weather, the MJO has proven very difficult to simulate with GCMs (e.g., Lin et al., 2008; Kim et al., 2009).

Inspired by the results of Grabowski and Smolarkiewicz, Khairoutdinov and Randall (2001) created a multiscale version of the Community Atmosphere Model (CAM; Collins et al., 2006). They disabled the parameterizations of the CAM, and replaced them with a simplified version of Khairoutdinov's CRM (Khairoutdinov and Randall, 2003). One copy of the CRM runs in each grid-column of the CAM. The CRM is two-dimensional (one horizontal dimension, plus the vertical), and uses periodic lateral boundary conditions. In the study of Khairoutinov and Randall (2001), the CRM had a horizontal domain 64 grid columns wide, with a horizontal grid spacing of 4 km.

Khairoutinov and Randall dubbed the embedded CRM a "super-parameterization." The *combination* of a GCM with a super-parameterization is now called a Multiscale Modeling

[2] The senior author of this paper first learned about the MJO and entraining plumes in classes taught by Prof. Michio Yanai.

Framework, or MMF, and the MMF based on the CAM is now called the "SP-CAM." A second MMF was created by Tao et al. (2009), using a different GCM and a different CRM. As of spring 2014, three more MMFs are being tested, each based on a different GCM.

Coupling the CRM and the GCM

Fig. 3 schematically illustrates the coupling of the embedded CRM with the GCM, as implemented in the SP-CAM. The GCM provides advective forcing to the CRM, much as observed advective forcing can be supplied to the "column physics" of a model that is being

Fig. 3: Schematic illustrating the coupling of the GCM and the CRM, in the SP-CAM.

tested in simulations based on field data (e.g., Randall et al., 1996). The CRM provides heating and drying as feedback to the GCM, just as any conventional parameterization would do.

The GCM's time step is typically tens of minutes, while the CRM's time step is on the order of ten seconds. It is assumed (and required) that the GCM's time step is an integer multiple of the CRM's time step. The CRM "sub-cycles" through a sequence of its short time steps, in order to determine the physical tendencies averaged over one of the longer GCM time steps. The CRM runs continuously throughout a simulation; it is not restarted between GCM time steps.

The coupling between the GCM and the CRM is very simple, and has some nice properties. It was used by Khairoutdinov and Randall (2001) and in all subsequent work with the SP-CAM. Here is how it works: Let q be a generic scalar variable that is defined in both the GCM and CRM. We write

$$\widetilde{q_G^{n+1}} \equiv q_G^n + B_G \Delta t_G \,, \tag{1}$$

so that

$$B_G = \frac{\widetilde{q_G^{n+1}} - q_G^n}{\Delta t_G} \,. \tag{2}$$

Here B_G is the adiabatic tendency of q due to non-CRM effects, as determined by the GCM; the subscript G denotes a GCM value; the superscripts n and $n+1$ denote successive GCM time steps; and Δt_G is the size of the GCM time step. The tilda on $\widetilde{q_G^{n+1}}$ denotes a provisional value. Eq. (1) represents a "partial time step," before the diabatic tendency of q is accounted for by the CRM.

The CRM variables, denoted by q_C, are updated using CRM time steps of size Δt_C:

$$\frac{q_C{}^{m+1} - q_C{}^{m}}{\Delta t_C} = B_C + \left(\frac{\widetilde{q_G{}^{n+1}} - \langle q_C \rangle^n}{\Delta t_G} \right) + S_C \,. \tag{3}$$

Here the superscripts m and $m+1$ denote successive CRM time steps. In (3), the term B_C represents the adiabatic tendency of q_C due to advection on the CRM's grid. Pointy brackets denote a horizontal average over the CRM's domain. The quantity $\langle q_C \rangle^n$ is the CRM-domain-average of q_C at the beginning of the GCM time step. The term $\left(\frac{\widetilde{q_G^{n+1}} - \langle q_C \rangle^n}{\Delta t_G} \right)$ is the mechanism through which the GCM's advective tendencies are felt by the CRM; in other words, it represents the forcing of the CRM by the GCM. The forcing is held constant as the CRM sub-cycles through one GCM time step, and it is also independent of horizontal position on the CRM's grid. The source of q due to the CRM physics is denoted by S_C, which has no counterpart in Eq. (1) because the physics is computed only in the CRM, not in the GCM.

We take enough CRM time steps to span the longer GCM time step, finally arriving at GCM time level $n+1$. Then we let the CRM feed back on the GCM. To implement the feedback, the GCM variables are updated using

$$\begin{aligned} \frac{q_G^{n+1} - q_G^n}{\Delta t_G} &= B_G + \frac{\langle q_C \rangle^{n+1} - \widetilde{q_G^{n+1}}}{\Delta t_G} \\ &= B_G + \frac{\langle q_C \rangle^{n+1} - \left(q_G^n + B_G \Delta t_G \right)}{\Delta t_G} \\ &= \frac{\langle q_C \rangle^{n+1} - q_G^n}{\Delta t_G} \,. \end{aligned} \tag{4}$$

Here $\langle q_C \rangle^{n+1}$ represents the horizontal average of q_C at GCM time level $n+1$, i.e., at the end of the sequence of CRM time steps based on (2).

Comparing the left-hand side of (4) with the third line on the right-hand side, we see that

$$q_G^{n+1} = \langle q_C \rangle^{n+1} . \tag{5}$$

Of course, we can also write

$$q_G^{n} = \langle q_C \rangle^{n} . \tag{6}$$

The implication is that, at both the beginning and end of the GCM's time step, the GCM's value of q_G is guaranteed to agree with the horizontal average of the CRM values. The two models cannot "drift apart."

Use of (1) in (3) shows that the CRM variables evolve according to

$$\frac{{q_C}^{m+1} - {q_C}^{m}}{\Delta t_C} = B_C + B_G + S_C . \tag{7}$$

This means that the CRM feels the GCM advection as a simple additive term. If we horizontally average (7) over the CRM's grid, we get

$$\frac{\langle q_C \rangle^{m+1} - \langle q_C \rangle^{m}}{\Delta t_C} = \langle B_C \rangle + B_G + \langle S_C \rangle . \tag{8}$$

The CRM's periodic lateral boundary conditions imply that $\langle B_C \rangle$ involves only vertical transports. Finally, from (5), (6), and (8), we see that

$$\frac{{q_G}^{n+1} - {q_G}^{n}}{\Delta t_G} = B_G + \overline{\langle B_C + S_C \rangle}, \tag{9}$$

where the overbar on the right-hand side represents an average over the GCM time step. The interpretation of (9) is simple and clear.

The key points to take away from the discussion above are that the coupling strategy represented by (1-3) leads to the result (9), and also guarantees (5) and (6). The coupling strategy

therefore guarantees consistency between the GCM fields and the CRM fields, as they co-evolve during a simulation. See Grabowski (2004) for further discussion.

The CRM uses the anelastic system of equations with height as the vertical coordinate (Khairoutdinov and Randall, 2003), while GCM uses the quasi-hydrostatic system with the terrain-following sigma-pressure coordinate (Collins et al., 2006). For each GCM grid column, the time-varying GCM sounding is used as the "reference sounding" in the anelastic system of the CRM. When the CRM is called by the GCM, it receives as input the provisional temperature and vapor profiles that have been updated by the GCM dynamics, as well as the height and pressure profiles. The CRM adjusts its vertical grid to agree with the GCM's, assuming that the reference-state pressures at mid- and interface-levels are the same as the GCM's. The CRM computes the reference-state air density from hydrostatic balance.

The heights of the GCM's grid levels are slightly different from those on the previous GCM time step, so there is a small spike at the beginning of each CRM subcycle, but because the grid height in the GCM evolves slowly, the spike does not significantly affect the CRM results.

At the beginning of a sequence of CRM time steps, the vertical integral of water vapor in the CRM is not the same as it was when the CRM finished the preceding sequence. This discrepancy is eliminated at the end of CRM call, however, because it is automatically corrected by the prescribed large-scale forcing. As a result, the vertical integral of total water in the CRM at the end of the GCM time step always equals the vertical integral of total water in the GCM after the provisional dynamics step, minus the precipitation that falls out during the CRM time steps. A similar result holds for the frozen static energy.

A complication is that water in the form of falling precipitation inside the grid columns of the CRM is not passed back to GCM at the end of the sequence of CRM time steps; some of the precipitation remains in the CRM grid, "hanging in the air." Although such hanging precipitation is not accounted for by the GCM, it is conserved by the CRM, and can eventually reach the surface and be accounted for as rainfall, or else return to vapor through evaporation or sublimation.

Because the CRM is two-dimensional, we do not permit momentum feedback to the GCM winds. This means that the model cannot simulate the effects of vertical momentum transport by convection and gravity waves that are resolved on the CRM's grid (Khairoutdinov et al., 2005). We return to this point later.

Further discussion of the super-parameterization and how it differs from conventional parameterizations is given near the end of this chapter. We now turn to an overview of results that have been produced through the use of the super-parameterization.

Simulations of tropical variability

Many investigators have published the results of studies based on the SP-CAM, in more than 50 refereed journal articles. A recurring theme of these studies has been modes of variability in the climate system. In order of increasing time scale, the types of variability considered so far include the diurnal cycle (Khairoutdinov et al., 2005; Pritchard and Somerville, 2009 a, b; Pritchard et al., 2011; Kooperman et al., 2013), easterly waves and tropical cyclones (McCrary, 2012; Stan, 2012), fluctuations of the Asian summer monsoon (DeMott et al., 2011, 2013) and

the Madden-Julian Oscillation (Benedict and Randall, 2009, 2011; Thayer-Calder and Randall, 2009; Kim et al., 2009; Andersen and Kuang, 2012; and Arnold et al., 2013), El Niño and the Southern Oscillation (Stan et al., 2010), and anthropogenic climate change (Wyant et al., 2006, 2012; Stan et al., 2014; Arnold et al., 2014). Here we provide a value-added overview of some of these results, with an emphasis on the effects of coupling the SP-CAM to an ocean model.

The diurnal cycle of precipitation

Solar heating and nocturnal cooling of the land surface are associated with a vigorous diurnal cycle of convective activity over the warm continents of the tropics and the summer hemisphere midlatitudes, with a maximum in late afternoon or early evening (e.g., Dai, 2001). Many global models fail to simulate the observed afternoon maximum (Dai, 2006; Dirmeyer et al., 2011). Khairoutdinov et al. (2005, their Fig. 13) pointed out that the SP-CAM produces fairly realistic diurnal cycles of precipitation over both the continents and the oceans. Pritchard and Somerville (2009 a, b) Pritchard et al. (2011), and Kooperman et al. (2013) performed detailed analyses of the SP-CAM's simulations of the diurnal cycle of precipitation over central North America in summer. They showed that the model is able to simulate the observed propagation of diurnally forced convective systems from near the Rocky Mountains in the afternoon to near Omaha after midnight. An example is shown in Fig. 4, which depicts rapid eastward propagation of diurnally excited convective disturbances in both the observations and the SP-CAM, but not in the CAM.

The afternoon precipitation maximum over land is driven by solar heating of the ground, which leads to increasing sensible and latent heat fluxes from early morning until mid afternoon. These energy fluxes directly modify the the thermodynamic properties of the boundary layer. All models include these basic physical processes. In order to produce a realistic diurnal cycle of precipitation, however, deep convective clouds must respond realistically to the changing thermodynamic properties of the boundary layer. The coupling of the parameterized boundary layer with the parameterized deep convection is therefore key to the ability of a model to simulate the diurnal cycle of precipitation over heated land. This coupling includes the lofting of boundary layer air to form cumulus clouds in the free atmosphere, and the production of cold pools by precipitation-driven downdrafts that penetrate into the boundary layer. In many existing GCMs, the boundary layer and cumulus parameterizations have been developed independently, their coupling is perfunctory, and the processes mentioned above are either not explicitly formulated or missing altogether. Many models include rather arbitrary assumptions about "triggers" that enable the development of deep convection, e.g., the requirement of a minimum relative humidity in the boundary layer.

The situation is very different with SP-CAM, in which the "boundary layer parameterization" of the GCM is limited to a parameterization of the surface fluxes. Turbulent transport above the surface is computed on the CRM's relatively high-resolution grid, and includes both resolved and parameterized components. The coupling of the boundary layer with the cumulus layer is explicitly resolved, and does not rely on parameterizations, perfunctory or otherwise. Cumulus clouds form when warm, humid air near the surface is lofted by the vertical motion resolved on the CRM's grid. Downdrafts resolved on the CRM's grid can produce cold

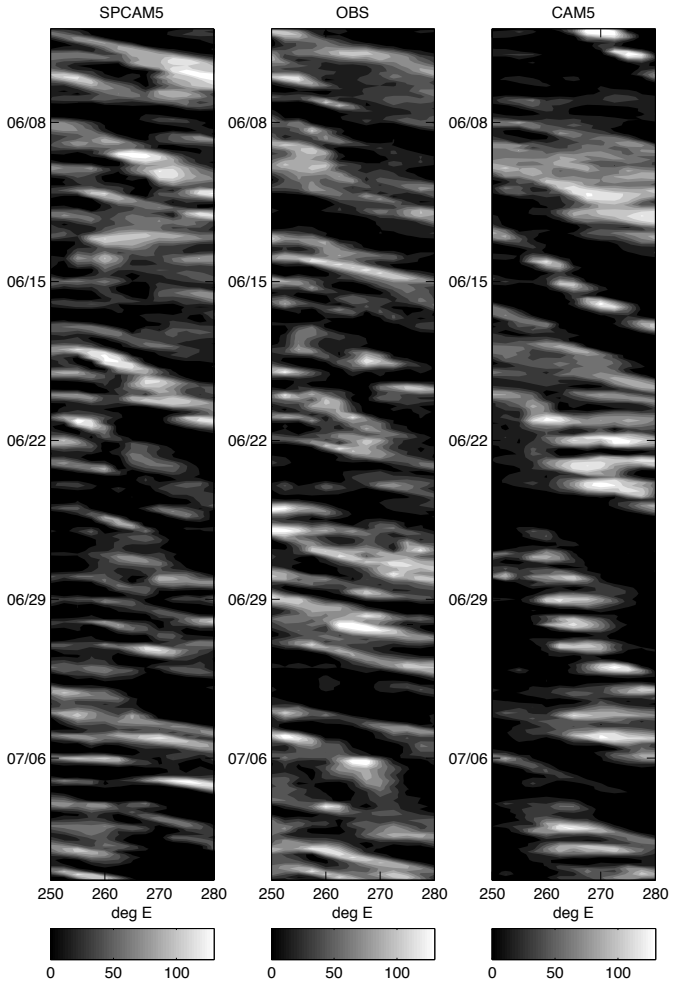

Fig. 4: Time-longitude structure of warm season diurnal convective activity in the lee of the Rocky Mountains between 35˚N and 45˚N, and plotted for longitudes between 250˚ and 280˚ E. Each panel shows the longwave cloud forcing, bandpass filtered to include periods between 12 and 48 hours, plotted over a period of 30 days.The left panel shows SP-CAM5, the center panel shows observations, and the right panel shows CAM5. Based on Kooperman et al. (2013).

pools in the boundary layer. These processes are poorly resolved because of the CRM's 4-km horizontal grid spacing, but the results suggest that an explicit representation with poor resolution can be more successful than a current-generation parameterization.

The Great Red Spot

Early work with the SP-CAM was based on the use of prescribed seasonally varying sea surface temperatures (SSTs). As first pointed out by Khairoutdinov and Randall (2001), the SP-CAM produces an unrealistically active hydrologic cycle over the western North Pacific Ocean

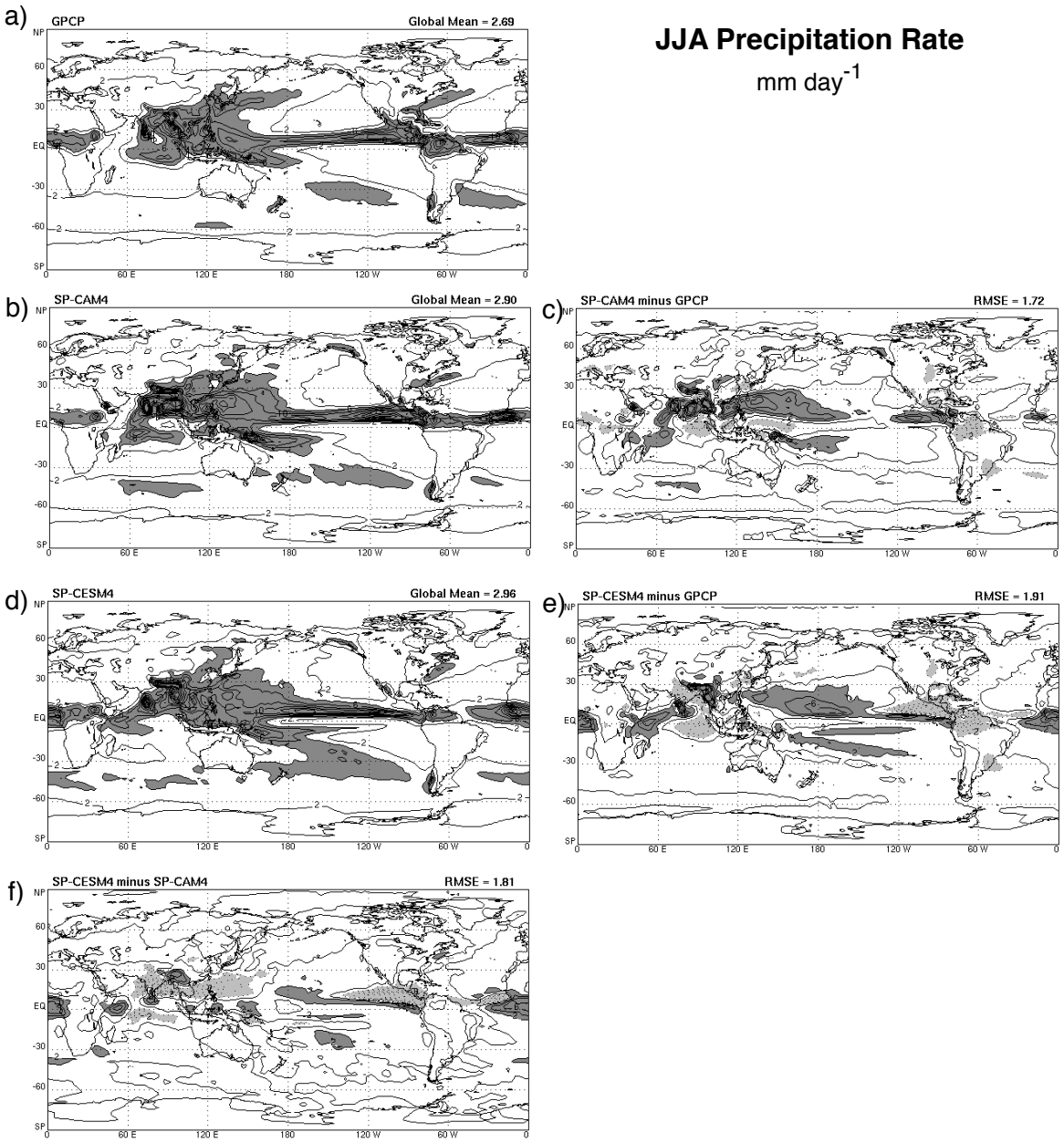

Fig. 5: (a) The observed climatological precipitation rate for July. (b) The simulated climatological precipitation rate for the SP-CAM. (c) The difference between the SP-CAM results and the observations. (d) The simulated climatological precipitation rate for the coupled ocean-atmosphere model, SP-CCSM. (e) The difference between the SP-CESM results and the observations. (f) The difference between the SP-CESM results and the SP-CAM results. Adapted from Stan et al. (2010). For precipitation rate maps, the contour interval is 2 mm day^{-1}, and values larger than 4 mm day^{-1} are shaded. For the difference maps, the contour interval is again 2 mm day^{-1}, values larger than 2 mm day^{-1} have dark shading, and values smaller than -2 mm day^{-1} have light shading.

during the northern summer months (Fig. 5c). The precipitation rate is unrealistically high, the precipitable water is excessive, the surface pressure is lower than observed, and the cyclonic low-level winds are too strong. The problem appears as an unrealistic eastward extension of the

Asian summer monsoon, which also produces excessively strong monsoon precipitation. It does not occur at other times of year. Because color plots of this phenomenon typically show strong red features over the western North Pacific Ocean, we call it the Great Red Spot (GRS). Interestingly, the MMF created by Tao et al. (2009) also produces a GRS, even though it is based on a different GCM and a different CRM.

A comparison of panels (b) and (d) of Fig. 5 shows that the GRS disappears when the SP-CAM is coupled with an ocean model. This was discovered when Stan et al. (2010) coupled the SP-CAM to a low-resolution version of POP (the Parallel Ocean Program); we call this coupled model the SP-CCSM[3]. As reported by Stan et al. (2010), and further analyzed by DeMott et al. (2011, 2013, 2014), the SP-CCSM gives a more realistic simulation of the atmospheric circulation than the SP-CAM "right out of the box," *without any tuning*, a somewhat surprising result in view of earlier experiences of others (e.g., Saussen et al., 1988). Besides eliminating the GRS, the SP-CCSM also produces a more realistic simulation of the Asian summer monsoon. In addition, Stan et al. (2010) found that the coupled model gives a more realistic simulation of El Niño, La Niña, and the Southern Oscillation, relative to the same coupled model with conventional atmospheric parameterizations.

The price paid for these improved results is a error in the simulated SST distribution. The error takes the form of a cooling in many locations (not shown), with a root-mean-square (RMS) value of 2.08 K. This is actually slightly smaller than the RMS error of the SST in version 3 of the conventionally parameterized CCSM, which also tends to produce tropical SSTs that are cooler than observed.

In the uncoupled model, the prescribed SSTs represent an effectively infinite reservoir of sensible and latent heat, which is unaffected by what happens in the simulated atmosphere. The strong cyclonic winds of the GRS promote intense evaporation, which supplies energy to maintain the GRS, as discussed by Luo and Stephens (2006). In the coupled model, the surface winds cool the SSTs, and this negative feedback prevents the development of the GRS. We can interpret the GRS as an error that comes from failure to include air-sea interactions in the uncoupled model.

[3] The CCSM is the Community Climate System Model, which has recently been re-named as the Community Earth System Model (CESM). The SP-CCSM is a version of the CCSM that uses SP-CAM as its atmospheric component.

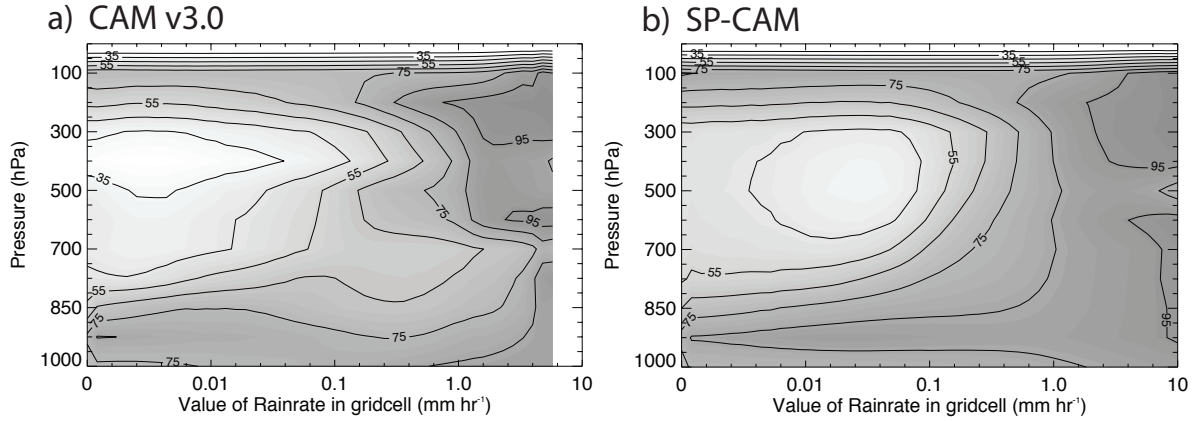

Fig. 6: Composite profiles of relative humidity binned by daily average rain rate in the region from 15ºS to 15ºN, and from 50ºE to the Date Line . The contour interval is 10%, and the 70% contour is heavy. From Thayer-Calder and Randall (2009).

The MJO

The ability of the SP-CAM to simulate the MJO was first reported by Khairoutdinov and Randall (2001), although Grabowski (2001) found something similar in a simplified global model. An extensive and generally favorable comparison of the simulated MJO with observations was reported by Benedict and Randall (2009). Thayer-Calder and Randall (2009) analyzed the relationship between water vapor and precipitation rate in the SP-CAM, and compared with version 3 of the conventionally parameterized CAM. They showed that in the SP-CAM heavy rainfall is accompanied by a very humid troposphere, while in version 3 of the CAM the lower troposphere remains dry even during intense rainfall (Fig. 6). They argued that a prerequisite for a realistic simulation of the MJO is that water vapor must exhibit a realistically large dynamic range. As discussed by Derbyshire et al. (2004) and others, deep convection may be unable to form unless the middle troposphere becomes sufficiently moist. This moistening is created by the convection itself. There are thus two separate issues: On the one hand, the simulated middle troposphere must become humid enough to permit realistic deep convection. On the other hand, the parameterized convection must be capable of moistening the middle troposphere. We return to this point later.

The analysis of Benedict and Randall (2009) shows that it is possible to produce a reasonably successful simulation of the MJO without taking into account the effects of air-sea interactions. Nevertheless, it is interesting to examine the effects of air-sea coupling on the MJO. Benedict and Randall (2011) used a slab ocean model (SOM) to study the effects of air-sea interactions on the MJO in a simplified framework. In the SOM, departures of the net surface energy flux from climatology can create sea surface temperature (SST) anomalies, depending on a prescribed ocean mixed layer depth, but the SST anomalies are damped with a 50-day time scale to keep the SSTs of the SOM close to those of a control run. As shown in Fig. 7, the air-sea interactions promote coherent eastward propagation of the MJO. The air-sea interactions also strengthen the coupling between dynamics, as represented by the 850 hPa zonal wind, and moist processes, as represented by the precipitation rate at 90°E.

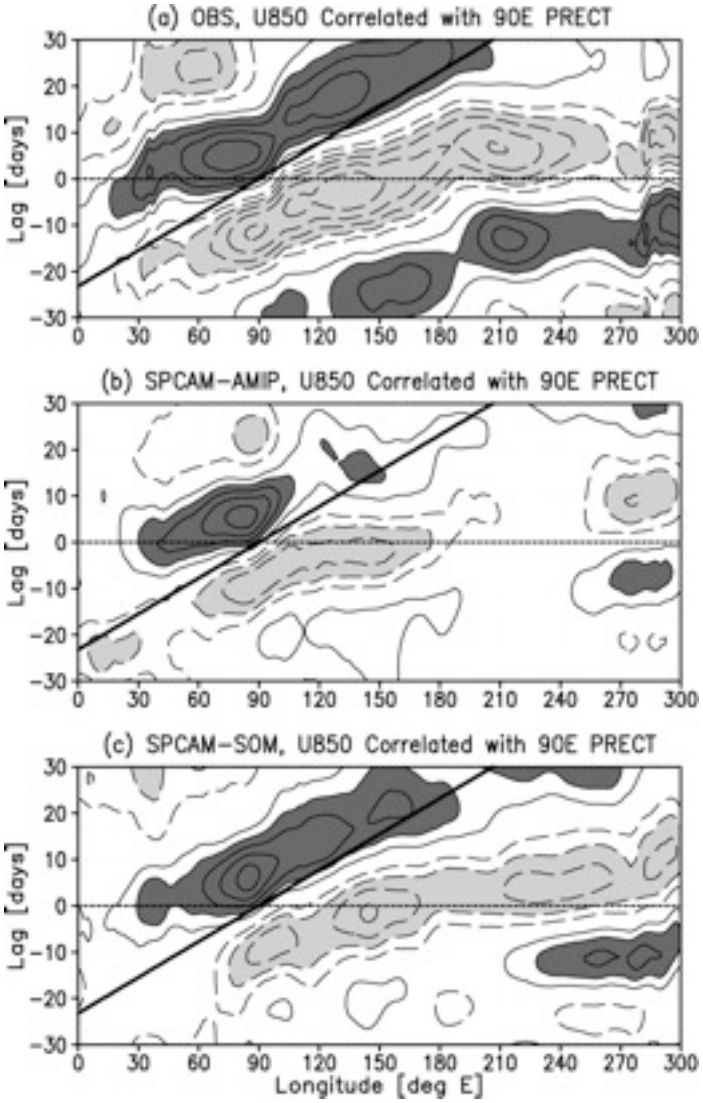

Figure 7: Correlations of the lagged 850 zonal wind with equatorial rainfall at 90°E for: (a) observations (ERA-Interim and GPCP), (b) SPCAM with prescribed seasonally varying sea surface temperatures, and (c) SPCAM-SOM. All fields are filtered to pass only MJO time scales, and merdionally averaged near the Equator. The horizontal axis is longitude relative to the Greenwich meridian, and the vertical axis is lag in days relative to the time of maximum precipitation at 90°E. The 5 m s^{-1} phase speed is shown with a thick black line. The contour interval is 0.1, with positive contours solid, negative contours dashed, and the zero contour omitted. Dark (light) gray shading denotes correlations greater than 0.2 (less than –0.2). Adapted from Benedict and Randall (2011).

.

In an analysis of results from their fully coupled model, Stan et al. (2010) also found that the air-sea interactions improve the realism of the simulated MJO, Fig. 8 shows the variance of precipitation in the range of frequencies and wave numbers associated with the MJO, plotted as a function of longitude, from the western Indian Ocean to the central Pacific. In the uncoupled SP-CAM, the simulated variance takes large values not only west of the Date Line, as observed, but also considerably further east. In the SP-CCSM, the simulated variance decreases realistically to the west of the Date Line. Further analysis of the results shows that the excessive variance in the SP-CAM results is found mainly in the region of the GRS. The elimination of the GRS in the coupled model leads to the more realistic variance distribution in SP-CCSM.

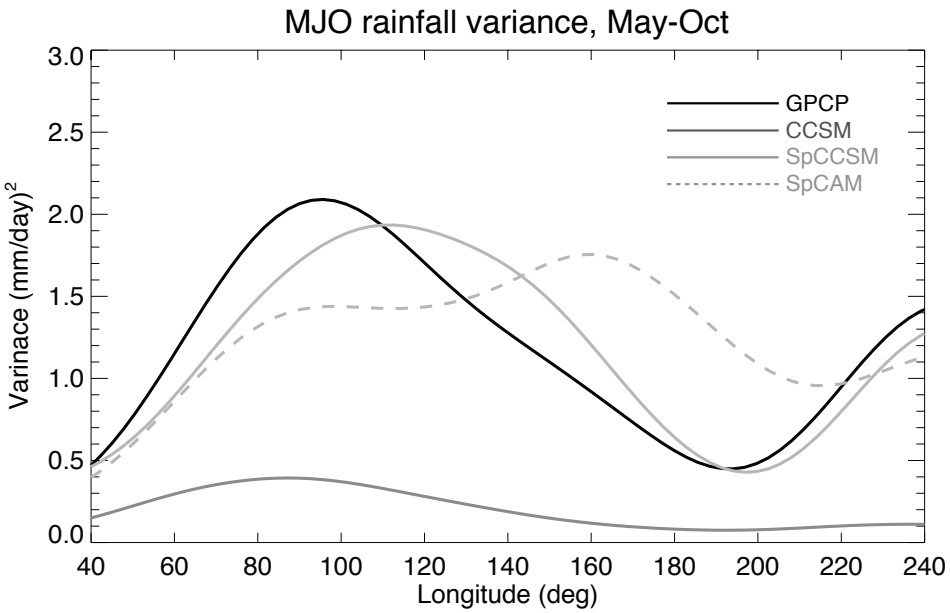

Figure 8: May-October MJO precipitation variance as a function of longitude for GPCP, SP-CCSM3, SP-CAM3, and CCSM3. Precipitation is filtered to retain 20-100 day variability and eastward-propagating wave numbers 1-6. Data are averaged from 5-25ºN.

Yanai waves

Wheeler-Kiladis diagrams (Wheeler and Kiladis, 1999) are ubiquitous now, but are most commonly shown only for modes that are symmetrical across the Equator, such as the MJO and

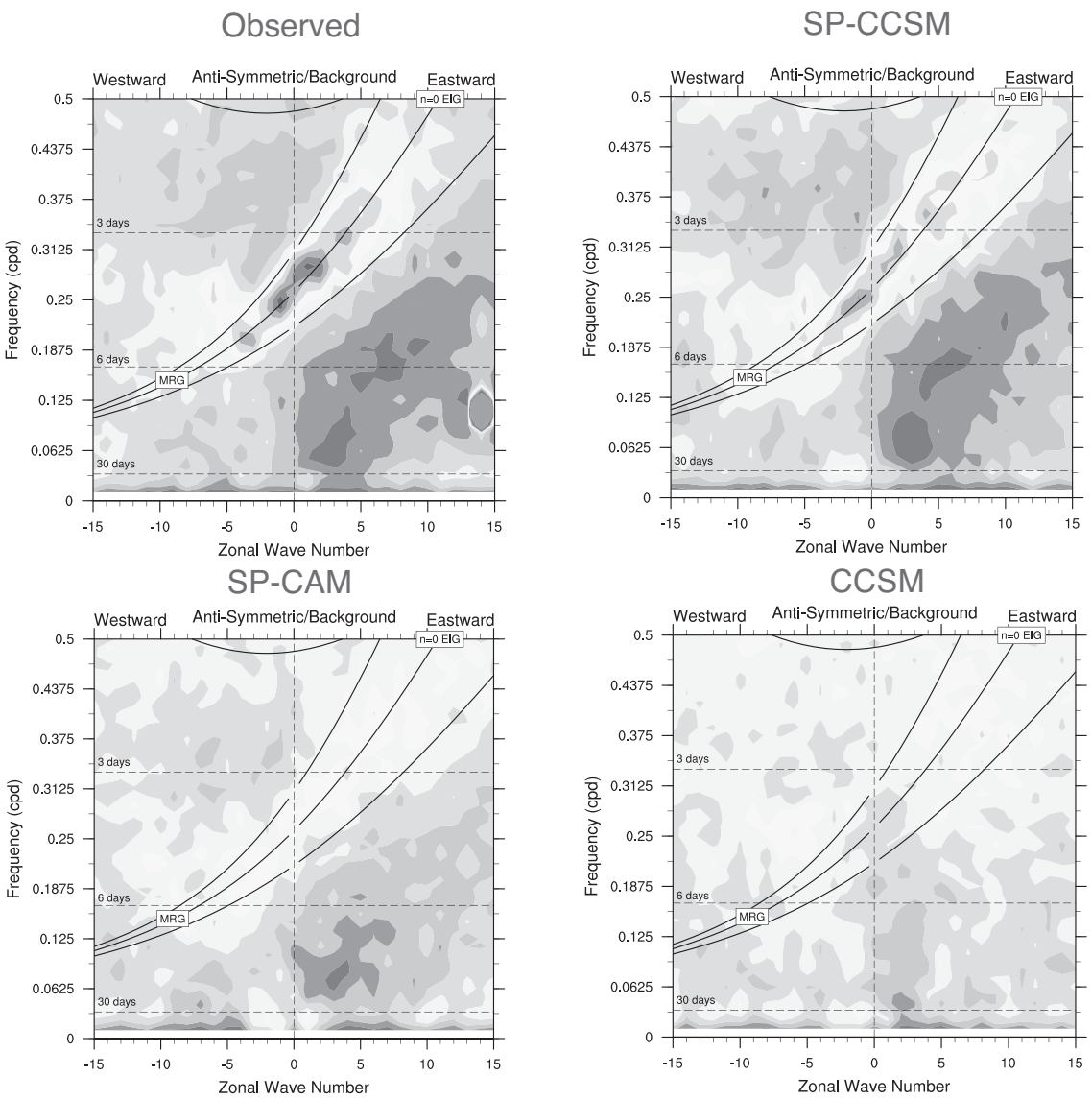

Figure 9: Signal-to-noise ratio of equatorially-antisymmetric component of OLR in observations, SPCCSM3, SPCAM3, and CCSM3. The dispersion relation for typical equivalent depths are indicated by solid lines. The "observed" feature near zonal wave number 15 and frequency 0.12 day^{-1} is spurious, and arises from aliasing of the satellite data. Here "MRG" refers to mixed Rossby-gravity waves, and "EIG" refers to eastward inertial-gravity waves.

Kelvin waves. Fig. 9 shows the *antisymmetric* power, which includes the westward-propagating Yanai waves[4]. The SP-CCSM produces a realistic level of Yanai-wave activity, while the SP-CAM generates considerably less. This improvement in the coupled model is due to a more realistic "basic state," relative to the uncoupled model, as discussed by DeMott et al. (2011).

[4] Also called mixed Rossby-gravity waves.

Monsoons

The Asian summer monsoon and its sub-seasonal variability attracted the attention of Prof. Yanai and his students (Luo and Yanai, 1983, 1984; He et al., 1987; Yanai and Li, 1994; Li and Yanai, 1996; Hung et al. 2004). Recently, DeMott et al. (2011, 2013) have investigated the ability of the SP-CAM and the SP-CCSM to simulate these important tropical weather systems. Fig. 10

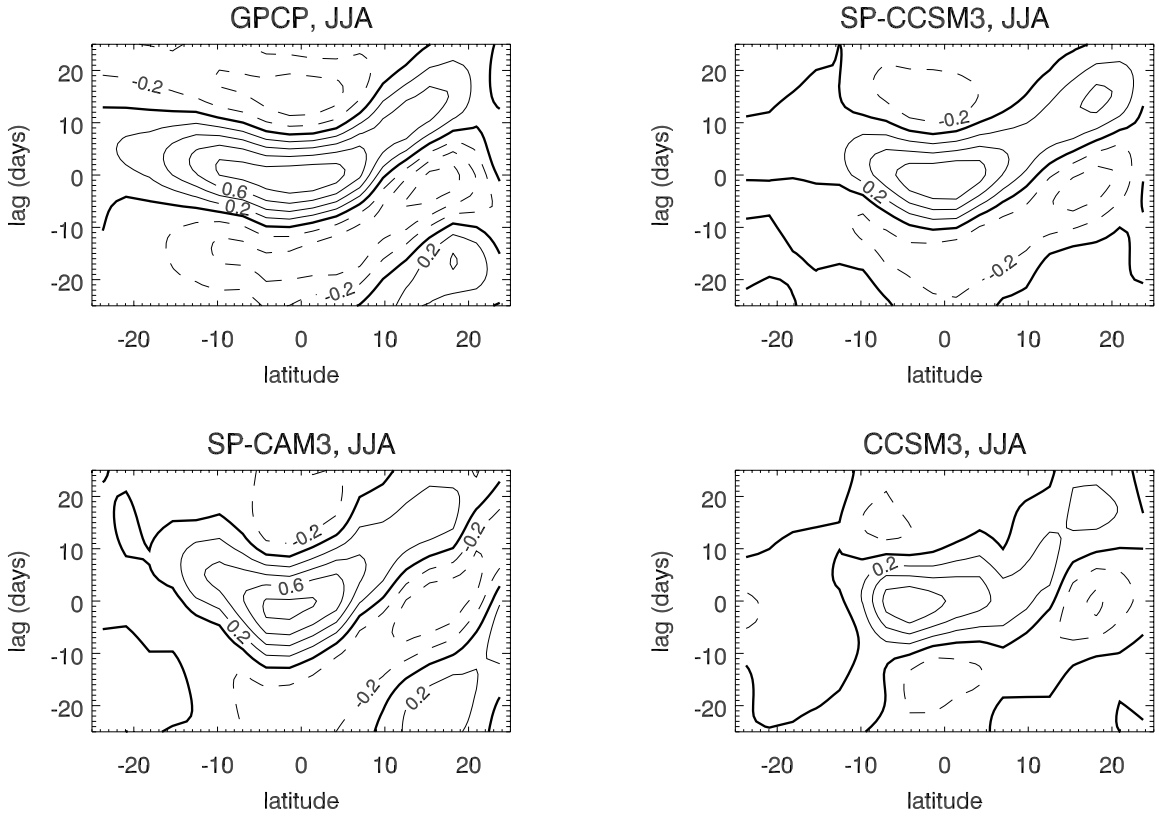

Figure 10: JJA lag-correlation of 20-100 day filtered precipitation with itself in GPCP, SP-CCSM, SP-CAM, and CCSM. The "3" on the end of SP-CCSM3 and SP-CAM3 and CCSM3 refers to version 3 of the CAM, which was used as the GCM in these simulations. The base point time series is the filtered precipitation averaged over 10ºS-5ºN, 80º-100ºE. The contour interval is 0.2, with positive (negative) values shown with solid (dashed) lines.

shows the northward propagation (and also the weaker southward propagation) of precipitation anomalies that occur during the Asian summer monsoon. Both the SP-CAM and the SP-CCSM produce somewhat realistic northward propagation. The mechanisms of this variability are discussed in detail by DeMott et al. (2013).

Recently, McCrary (2012) has investigated the ability of the SP-CAM and the SP-CCSM to simulate the African summer monsoon and the associated African Easterly Waves, which are

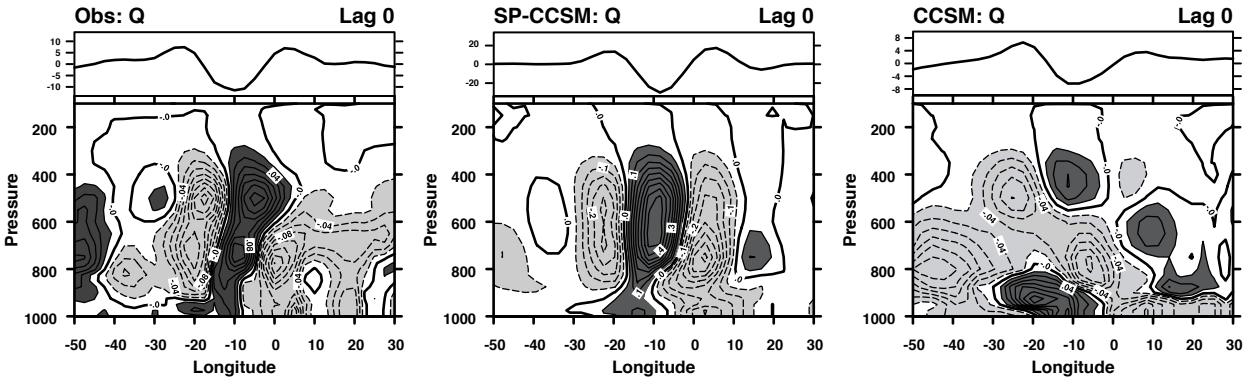

Figure 11: Longitude-height cross section of the specific humidity anomaly in African Easterly Waves as observed (left), as simulated by the SP-CCSM (middle) and as simulated by CCSM3 (right). The latitude is 10ºN. Units are g kg^{-1}. The heavy contour is zero, dashed contours are negative (lightly shaded) and solid contours are positive (darkly shaded). The contour interval for the SP-CCSM results is 0.05 g kg^{-1}, while the contour interval for the observations and for CCSM is 0.02 g kg^{-1}. The small plots at the top of each panel show anomalies of the outgoing longwave radiation, in W m^{-2}. The anomalies of both water vapor and outgoing longwave radiation are relative to seasonal means. Based on the work of McCrary (2012).

precursors to Atlantic tropical cyclones. Fig. 11 shows the phase relationship between the vertically varying water vapor mixing ratio and the precipitation maximum associated with composite African Easterly Waves. The SP-CCSM correctly produces a very moist troposphere at the time of maximum rainfall, but the conventionally parameterized CAM 3 produces a very unrealistic dry layer in the middle troposphere. This is strongly reminiscent of the earlier result of Thayer-Calder and Randall (2009), shown in Fig. 6, and suggests that the ability of models to produce realistic variations of water vapor is important not only for the MJO, but also for higher-frequency tropical disturbances. McCrary (2012) also shows that the SP-CCSM produces a somewhat realistic modulation of the African Easterly Waves by the MJO.

Concluding remarks

Parameterizations forever!

The results summarized in this paper demonstrate that super-parameterization can simulate a wide variety of tropical variability more realistically than today's conventionally parameterized models. We are confident[5], however, that future parameterizations can and will perform as well as or better than today's super-parameterizations. Our hope is that work with super-parameterizations can make that future happen sooner.

Apart from their practical use in simulations, parameterizations encapsulate our understanding of the way in which the parameterized physical processes interact with the large-scale circulation. Even with very successful simulations of tropical variability from global cloud-resolving models, we would need parameterizations, coupled with simplified models, to understand why the simulations succeeded.

[5] Modelers have to be optimistic!

Compared to what?

It is easy to criticize the super-parameterization. The CRM is two-dimensional. The 4-km horizontal grid spacing that is typically used in the CRM is too coarse to accurately resolve even large cumulus clouds. The periodic boundary conditions are unrealistic. Given these weaknesses of the approach, why does super-parameterization work so well?

To answer this question, it is useful to review the key differences between an MMF and a conventionally parameterized GCM. First of all, the CRM used in an MMF simulates cloud dynamics by explicitly solving the (two-dimensional) equation of motion, thus tying back to the "basic physics" developed by Isaac Newton and others. In contrast, conventional GCMs parameterize all of the dynamical processes associated with cloud growth and decay. For example, most cumulus parameterizations represent cumulus clouds as one-dimensional entraining plumes (e.g., Arakawa and Schubert, 1974). While it is true that the periodic lateral boundary conditions of the CRM are unrealistic, conventional parameterizations are so crude that the subject of lateral boundary conditions never even comes up.

In an MMF, the CRM simulates convective entrainment crudely but directly through its subgrid turbulence parameterization in combination with the simulated wind field resolved on the CRM grid. In contrast, entraining plume models often assume that the fractional entrainment rate is constant with height, which is in conflict with recent studies (e.g., Lin and Arakawa, 1997 a, b), or else they rely on entrainment parameterizations (e.g., Gregory, 2001; Chikira and Sugiyama, 2010).

Because the CRM solves the equation of motion, an MMF has no need for closure assumptions (e.g., quasi-equilibrium), nor does it use assumptions about triggers that initiate cloud formation. In addition, the CRM explicitly simulates some aspects of mesoscale organization, such as aggregation or squall lines; conventional parameterizations omit these processes entirely.

The CRM relies on questionable parameterizations of microphysics, turbulence, and radiative transfer. Of course, conventional models must also parameterize these same processes. A key difference, however, is that the CRM provides relatively detailed information as input to the parameterizations. For example, the CRM explicitly simulates (relatively) small-scale vertical velocities that can be used by microphysics parameterizations, whereas conventional parameterizations can only estimate cloud-scale vertical velocities using the entraining plume model. The CRM simulates small-scale shear and buoyancy fluctuations that are key input to turbulence parameterizations. Last but not least, the CRM explicitly simulates fractional cloudiness and cloud overlap, which are critical inputs to a radiation parameterization.

In addition, the CRM is a nonlinear fluid-dynamical model that exhibits *sensitive dependence on initial conditions*, i.e., it behaves chaotically, as does the real atmosphere (e.g., Hohenegger et al., 2006). As a result, the CRM-grid-averaged heating and drying rates that are passed to the GCM contain quasi-random components, which originate primarily on the smallest scales resolved by the CRM. In this sense, *the super-parameterization is a stochastic parameterization*. Efforts are under way to develop stochastic conventional parameterizations, but the super-parameterization generates stochastic heating and drying rates in a particularly natural way.

Finally, the SP-CAM is almost embarrassingly parallel, so that it can make efficient use of a very large number of processors. The reason is that the many copies of the CRM (one per CAM grid column) run independently, with no communication among themselves. As a result, for a given GCM grid spacing the SP-CAM can use many more processors than a conventionally parameterized model. Although the SP-CAM does hundreds of times more arithmetic per simulated day than a conventionally parameterized GCM with the same resolution, the ability of the MMF to utilize more processors than a conventional GCM means that the wall-clock time required to complete a given simulation with the super-parameterization is only moderately

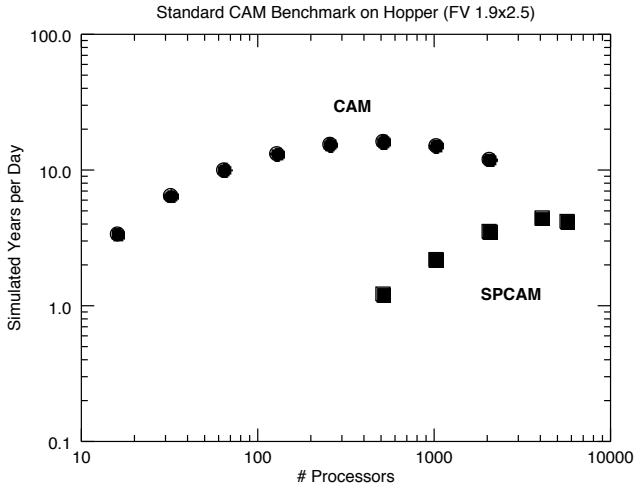

Fig. 12: Plots of simulated years per wall-clock day versus the number of processors used, for the conventional CAM (dots) and the SP-CAM (squares). The GCM grid spacing is 2.5º of longitude by 2º of latitude for both models. Note that the axes are logarithmically scaled. The figure shows that, with this resolution, the SP-CAM can efficiently use thousands of processors, while the CAM is limited to hundreds. The timing tests were performed on Hopper, a Cray XE6 at the National Energy Research Scientific Computer Center (NERSC), by Mark Branson of Colorado State University.

longer than that required with a conventional parameterization. An example is shown in Fig. 12. The SP-CAM is orders of magnitude less expensive than a global cloud-resolving model (GCRM; e.g., Tomita et al., 2005).

Process models and global models

Over the past two decades, cloud-parameterization testing has become organized on an international scale, beginning with NASA's[6] FIRE[7] program in the 1980s (Cox et al., 1987), and continuing in the 1990s and beyond with DOE's[8] ARM Program[9] (Stokes and Schwartz, 1994) and the GCSS[10] activities (Randall et al., 2003 b). One strategy for testing parameterizations is to drive both the parameterized column physics of a GCM and a high-resolution CRM with

[6] NASA is the National Aeronautics and Space Administration.

[7] FIRE was the First ISCCP Regional Experiment; ISCCP is the International Satellite Cloud Climatology Project.

[8] DOE is the U.S. Department of Energy.

[9] Atmospheric Radiation Measurement Program.

[10] GCSS was the GEWEX Cloud Systems Study; GEWEX was the Global Energy and Water Experiment. The work of GCSS is now continuing under the more general name GEWEX Atmospheric System Studies (GASS).

"forcing" data based on field observations, and then to inter-compare the results of the two models with additional observations from the field (Randall et al., 1996). The column-physics is called a "single-column model," and the high-resolution model is sometimes called a "process model."

An important limitation of this strategy is that, because single-column models and process models represent only a small regional domain, they cannot "feed back" to the large-scale circulation; the effects of the large-scale circulation are simply prescribed and non-interactive. This limitation is now breaking down. Both MMFs and global cloud-resolving models are

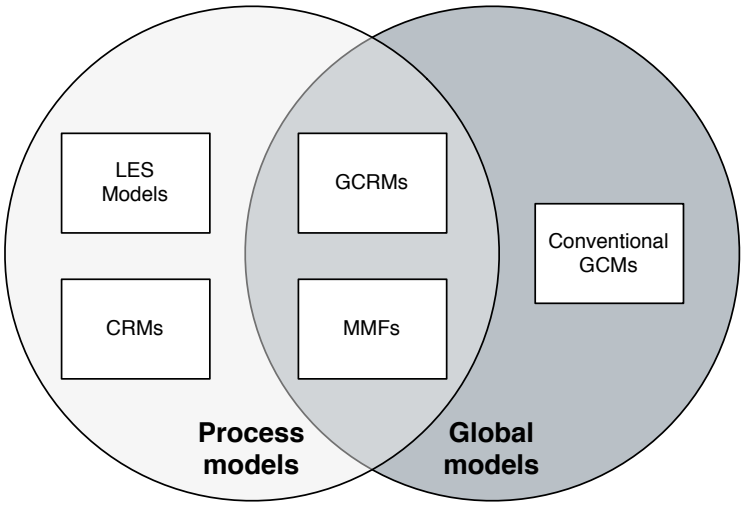

Figure 13: In this Venn diagram, the circle on the left represents process models, and the circle on the right represents global atmospheric models. Until recently, these two classes of models did not overlap. Today, as shown in the figure, there is some intersection in the form of GCRMs and MMFs. This figure first appeared in Randall (2013).

simultaneously global models *and* process models (Fig. 13).

Improving the MMF

There are many ways to improve the MMF by enhancing the CRM. Perhaps the highest priority is to incorporate better parameterizations of shallow clouds and turbulence that cannot be resolved on the CRM's grid. Higher-order closure methods have been developed for the CRM and tested in the MMF (Cheng and Xu, 2011, 2013; Xu and Cheng, 2013 a, b; Bogenschutz et al., 2012, 2014), with very promising results. These modern turbulence parameterizations predict (or diagnose) fractional cloudiness and the variability of temperature and water vapor at scales that are not resolved on the CRM's grid. With appropriate attention to coupling the parameterizations, this subgrid information can be used by improved parameterizations of microphysics (e.g., Morrison and Grabowski, 2007, 2008) and radiation (e.g., Pincus and Stevens, 2009). In addition, more advanced numerical methods have been implemented in the CRM (Yamaguchi et al., 2011). These various improvements are incremental, but very important.

More sweeping revisions of the MMF are also under development. The chapter of this book by Arakawa and colleagues describes a radically different "second-generation" MMF, called the

Q3D (Quasi-Three-Dimensional) MMF. The Q3D MMF partially removes the periodic boundary conditions of the CRM, and includes the dynamical effects of three-dimensionality in a simplified way, while still consuming much less computer time than a GCRM. We hope that, in the years to come, the Q3D MMF will open the door to exciting new studies of global and tropical dynamics.

Acknowledgments

The lead author was lucky enough to take all of the classes that Professor Michio Yanai offered in the early and middle 1970s. Prof. Yanai was a great teacher, a superb scientist, and a very kind, humble man.

Prof. Michael Pritchard of the University of California at Irvine provided Figure 4.

Initial development of the SP-CAM was supported by the U.S. Department of Energy through the ARM (Atmospheric Radiation Measurement) Program. More recently, the research has been supported by the National Science Foundation Science and Technology Center for Multi-Scale Modeling of Atmospheric Processes (CMMAP), managed by Colorado State University under cooperative agreement No. ATM-0425247.

References

Arnold, N. P., Z. Kuang, and E. Tziperman, 2013: Enhanced MJO-like Variability at High SST. *J. Climate*, **26**, 988-1001. doi: http://dx.doi.org/10.1175/JCLI-D-12-00272.1

Benedict, J. J., and D. A. Randall, 2009: MJO Structure in the Superparameterized CAM. *J. Climate,* **66**, 3277-3296.

Benedict, J. J., and D. A. Randall, 2011: Impacts of idealized air-sea coupling on Madden-Julian Oscillation structure in the super-parameterized CAM. *J. Atmos. Sci*., **68**, 1990-2008.

Bogenschutz, P. A., A. Gettelman, H. Morrison, V. E. Larson, D. P. Schanen, N. R. Meyer, and C. Craig, 2012: Unified parameterization of the planetary boundary layer and shallow convection with a higher-order turbulence closure in the community atmosphere model. *Geosci. Model Dev*., **5**, 1407–1423.

Bogenschutgz, P. A., A. Gettelman, H. Morrison, V. Larson, and C. Craig, 2014: Higher-Order Turbulence Closure and Its Impact on Climate Simulations in the Community Atmosphere Model. *J. Climate,* **26**, 9655–9676. doi: http://dx.doi.org/10.1175/JCLI-D-13-00075.1.

Cheng, A., and K.-M. Xu, 2011: Improved low-cloud simulation from a multiscale modeling framework with a third-order turbulence closure in its cloud-resolving model component. *J. Geophys. Res*., **116**, 19 pp. doi:10.1029/2010JD015362.

Cheng, A., and K.-M. Xu, 2013: Evaluating Low Cloud Simulation from an Upgraded Multiscale Modeling Framework Model. Part III: Tropical and Subtropical Cloud Transitions over the Northern Pacific. *J. Climate,***26**, 5761-5781.

Chikira, M., and M. Sugiyama, 2010: A Cumulus Parameterization with State-Dependent Entrainment Rate. Part I: Description and Sensitivity to Temperature and Humidity Profiles. *J. Atmos. Sci*., **67**, 2171-2193.

Collins, W. D., C. M. Bitz, M. L. Blackmon, G. B. Bonan, C. S. Bretherton, J. A. Carton, P. Chang, S. C. Doney, J. J. Hack, T. B. Henderson, J. T. Kiehl, W. G. Large, D. S. McKenna, B. D. Santer, and R. D. Smith, 2006: The Community Climate System Model Version 3 (CCSM3). *J. Climate*, **19**, 2122-2143.

Cox, S. K., D. McDougal, D. A. Randall, and R. A. Schiffer, 1987: FIRE - The First ISCCP Regional Experiment. *Bull. Amer. Meteor. Soc*., **68**, 114-118.

Dai, A., 2001: Global precipitation and thunderstorm frequencies. Part II: Diurnal variations. *J. Climate*, **14**, 1112-1128.

Dai, A., 2006: Precipitation characteristics in eighteen coupled climate models. *J. Climate*, **19**, 4606-4630.

DeMott, C. A., C. Stan, D. A. Randall, J. L. Kinter III, and M. Khairoutdinov, 2011: The Asian Monsoon in the Super-Parameterized CCSM and its relation to tropical wave activity. *J. Climate,* **24**, 5134-5156.

DeMott, C. A., C. Stan, and D. A. Randall, 2013: Northward Propagation Mechanisms of the Boreal Summer Intraseasonal Oscillation in the ERA-Interim Reanalysis and SP-CCSM. *J. Climate, 26,* 1973–1992. doi: http://dx.doi.org/10.1175/JCLI-D-12-00191.1

DeMott, C. A., C. Stan, D. A. Randall, and M. Branson, 2014: Intraseasonal Variability in Coupled GCMs: The Roles of Ocean Feedbacks and Model Physics. *J. Climate*. **27**, 4970-4994, doi: http://dx.doi.org/10.1175/JCLI-D-13-00760.1.

Derbyshire, S. H., I Beau,P. Bechtold, J.-Y. Grandpeix, J.-M. Piriou, J. L. Redelsperger, and P. M. M. Soares, 2004: Sensitivity of moist convection to environmental humidity. *Quart. J. Roy. Meteor. Soc.*, **130**, 3055-3079. doi: 10.1256/qj.03.130.

Dirmeyer, P. A., B. A. Cash, J. L. Kinter III, T. Jung, L. Marx, M. Satoh, C. Stan, H. Tomita, P. Towers, N. Wedi, D. Achuthavarier, J. M. Adams, E. L. Altshuler, B. Huang, E. K. Jin, and J. Manganello, 2011: Simulating the diurnal cycle of rainfall in global climate models: Resolution versus parameterization. *Clim. Dyn*., 20 pp., DOI 10.1007/s00382-011-1127-9.

Esbensen, S. K., L. J. Shapiro, and E. I. Tollerud, 1987: The Consistent Parameterization of the Effects of Cumulus Clouds on the Large-Scale Momentum and Vorticity Fields. *Mon. Wea. Rev.*, **115**, 664-669. doi: http://dx.doi.org/10.1175/1520-0493(1987)115<0664:TCPOTE>2.0.CO;2

Grabowski, W. W., and P. K. Smolarkiewicz, 1999: CRCP: A cloud resolving convection parameterization for modeling the tropical convective atmosphere. *Physica D*, **133**, 171-178.

Grabowski, W. W., 2001: Coupling cloud processes with the large-scale dynamics using the cloud-resolving convection parameterization (CRCP). *J. Atmos. Sci.*, **58**, 978-997.

Grabowski, W. W., 2004: An improved framework for superparameterization. *J. Atmos. Sci.*, **61**, 1940-1952.

Gregory, D., 2001: Estimation of entrainment rate in simple models of convective clouds. *Quart. J. Roy. Meteor. Soc*., **127**, 53-72.

He, H., J. W. McGinnis, Z. Song, and M. Yanai, 1987: Onset of the Asian Summer Monsoon in 1979 and the Effect of the Tibetan Plateau. *Mon. Wea. Rev.*, **115**, 1966-1995. doi: http://dx.doi.org/10.1175/1520-0493(1987)115<1966:OOTASM>2.0.CO;2

Hohenegger, C., D. Lüthi, and C. Schär, 2006: Predictability Mysteries in Cloud-Resolving Models. *Mon. Wea. Rev*., **134**, 2095-2107

Hung, C.-W., X. Liu, and M. Yanai, 2004: Symmetry and Asymmetry of the Asian and Australian Summer Monsoons. *J. Climate*, **17**, 2413-2426. doi: http://dx.doi.org/10.1175/1520-0442(2004)017<2413:SAAOTA>2.0.CO;2

Khairoutdinov, M. F., and D. A. Randall, 2001: A Cloud Resolving Model as a Cloud Parameterization in the NCAR Community Climate System Model: Preliminary Results. *Geophys. Res. Lett.*, **28**, 3617-3620.

Khairoutdinov, M., and D. A. Randall, 2003: Cloud-resolving modeling of ARM Summer 1997 IOP: Model formulation, results, uncertainties and sensitivities. *J. Atmos. Sci.*, **60**, 607-625.

Khairoutdinov, M., D. A. Randall, and C. A. DeMott, 2005: Simulation of the atmospheric general circulation using a cloud-resolving model as a super-parameterization of physical processes. *J. Atmos. Sci.*, **62**, 2136-2154.

Kim, D., K. Sperber, W. Stern, D. Waliser, I.-S. Kang, E. Maloney, W. Wang, K. Weickmann, J. Benedict, M. Khairoutdinov, M.-I. Lee, R. Neale, M. Suarez, K. Thayer-Calder, and G. Zhang, 2009: Application of MJO simulation diagnostics to climate models. *J. Climate*, **22**, 6413-6436.

Kooperman, G. J., M. S. Pritchard, and R. C. J. Somerville, 2013: Robustness and sensitivities of central U.S. summer convection in the super-parameterized CAM: Multi-model intercomparison with a new regional EOF index. *Geophys. Res. Lett.*, **40**, 3287–3291, doi: 10.1002/grl.50597.

Li, C., and M. Yanai, 1996: The Onset and Interannual Variability of the Asian Summer Monsoon in Relation to Land-Sea Thermal Contrast. *J. Climate*, **9**, 358-375. doi: http://dx.doi.org/10.1175/1520-0442(1996)009<0358:TOAIVO>2.0.CO;2

Lin, C., and A. Arakawa, 1997 a: The macroscopic entrainment processes of simulated cumulus ensemble. Part I: Entrainment sources. *J. Atmos. Sci.*, **54**, 1027-1043.

Lin, C., and A. Arakawa, 1997 b: Some bulk properties of cumulus ensembles simulated by a cloud-resolving model. Part II: Entrainment profiles. *J. Atmos. Sci.*, **56**, 3736-3748.

Lin, J., G. N Kiladis, B. E. Mapes, K. M. Weickmann, K. R. Sperber, W. Y. Lin, M. Wheeler, S. D. Schubert, A. Del Genio, L. J. Donner, S. Emori, J.-F. Gueremy, F. Hourdin, P. J. Rasch, E. Roeckner, and J. F. Scinocca, 2006. Tropical intraseasonal variability in 14 IPCC AR4 climate models. Part I: Convective signals. *J. Climate*, **19**, 2665-2690.

Luo, H., and M. Yanai, 1983: The Large-Scale Circulation and Heat Sources over the Tibetan Plateau and Surrounding Areas during the Early Summer of 1979. Part I: Precipitation and Kinematic Analyses. *Mon. Wea. Rev.*, **111**, 922-944. doi: http://dx.doi.org/10.1175/1520-0493(1983)111<0922:TLSCAH>2.0.CO;2

Luo, H., and M. Yanai, 1984: The Large-Scale Circulation and Heat Sources over the Tibetan Plateau and Surrounding Areas during the Early Summer of 1979. Part II: Heat and Moisture Budgets. *Mon. Wea. Rev.*, **112**, 966-989.doi: http://dx.doi.org/10.1175/1520-0493(1984)112<0966:TLSCAH>2.0.CO;2

Luo, J., and G. L. Stephens, 2006: An enhanced convection-wind-evaporation feedback in a superparameterization GCM (SP-GCM) depiction of the Asian summer monsoon. *Geophys. Res. Lett.*, **33**, L06707, doi:10.1029/2005GL025060.

Madden, R. A., and P. R. Julian, 1971: Detection of a 40-50 day oscillation in the zonal wind in the tropical Pacific. *J. Atmos. Sci.*, **28**, 702-708.

Madden, R. A., and P. R. Julian, 1972: Description of global scale circulation cells in the tropics with a 40-50 day period. *J. Atmos. Sci.,* **29,** 1109-1123.

McCrary, R. R., 2012: *Seasonal, Synoptic and Intraseasonal Variability of the West African Monsoon*. Ph.D. Dissertation, Colorado State University, 160 pp.

Morrison, H., and W. W. Grabowski, 2007: Comparison of Bulk and Bin Warm-Rain Microphysics Models Using a Kinematic Framework. *J. Atmos. Sci.*, **64**, 2839-2861. doi: http://dx.doi.org/10.1175/JAS3980.

Morrison, H., and W. W. Grabowski, 2008: A Novel Approach for Representing Ice Microphysics in Models: Description and Tests Using a Kinematic Framework. *J. Atmos. Sci.*, **65**, 1528-1548. doi: http://dx.doi.org/10.1175/2007JAS2491.1.

Pincus, R. and B. Stevens, 2009: Monte Carlo Spectral Integration: a consistent approximation for radiative transfer in large eddy simulations. J. *Adv. Model Earth Syst.*, **1**, 9. doi:10.3894/JAMES.2009.1.1.

Pritchard, M. S., and R. C. J. Somerville, 2009 a: Empirical orthogonal function analysis of the diurnal cycle of precipitation in a multi-scale climate model. *Geophys. Res. Lett.*, **36**, L05812, doi:10.1029/2008GL036964

Pritchard, M. S. and R. C. J. Somerville, 2009 b. Assessing the Diurnal Cycle of Precipitation in a Multi-Scale Climate Model. *J. Adv. Modeling Earth Syst.,* **1**, Art. 12.

Pritchard, Michael S., Mitchell W. Moncrieff, Richard C. J. Somerville, 2011: Orogenic Propagating Precipitation Systems over the United States in a Global Climate Model with Embedded Explicit Convection. *J. Atmos. Sci.*, **68**, 1821-1840. doi: http://dx.doi.org/10.1175/2011JAS3699.1

Randall, D. A., B. A. Albrecht, S. K. Cox, P. Minnis, W. Rossow, and D. Starr, 1995: On FIRE at Ten. *Adv. Geophys.*, **38**, 37-177.

Randall, D. A., K.-M. Xu, R. J. C. Somerville, and S. Iacobellis, 1996: Single-Column Models and Cloud Ensemble Models As Links Between Observations and Climate Models. *J. Climate*, **9**, 1683-1697.

Randall, D. A., M. Khairoutdinov, A. Arakawa, and W. Grabowski, 2003 a: Breaking the cloud-parameterization deadlock. *Bull. Amer. Meteor. Soc.*, **84**, 1547-1564.

Randall, D. A., J. Curry, P. G. Duynkerke, S. Krueger, B. Ryan, D. Starr, M. Miller, W. B. Rossow, and B. A. Wielicki, 2003 b: Confronting models with data: The GEWEX Cloud Systems Study. *Bull. Amer. Meteor. Soc.,* **84**, 455-469.

Randall, D. A., 2013: Beyond deadlock. *Geophys. Res. Lett.,* **40**, 1-7, doi: 10.1002/2013GL057998.

Saussen, R., K. Barthel, and K. Hasselmann, 1988: Coupled ocean-atmosphere models with flux correction. *Clim. Dyn.*, **2**, 145-163.

Stan, C., M. Khairoutdinov, C. A. DeMott, V. Krishnamurthy, D. M. Straus, D. A. Randall, J. L. Kinter, III, and J. Shukla, 2010: An ocean-atmosphere climate simulation with an embedded cloud resolving model. *Geophys. Res. Lett.*, **37**, L01702, doi: 10.1029/2009GL040822.

Stan, C., 2012: Is cumulus convection the concertmaster of tropical cyclone activity in the Atlantic? *Geophys. Res. Lett.*, **39**, doi:10.1029/2012GL053449.

Stan C., and L Xu. 2014: Climate Simulations and Projections with a Super-Parameterized Climate Model. *Environmental Modelling & Software*, **60**:134-152. DOI:10.1016/j.envsoft. 2014.06.013.

Sui, C.-H., and M. Yanai, 1986: Cumulus Ensemble Effects on the Large-Scale Vorticity and Momentum Fields of GATE. Part I: Observational Evidence. *J. Atmos. Sci.*, **43**, 1618-1642.

Sui, C.-H., M.-D. Cheng, X. Wu, and M. Yanai, 1989: Cumulus Ensemble Effects on the Large-Scale Vorticity and Momentum Fields of GATE. Part II: Parameterization. *J. Atmos. Sci.*, **46**, 1609-1629. doi: http://dx.doi.org/10.1175/1520-0469(1989)046<1609:CEEOTL>2.0.CO;2

Tao, W.-K., J. Chern, R. Atlas, D. A. Randall, X. Lin, M. Khairoutdinov, J.-L. Li, D. E. Waliser, A. Hou, C. Peters-Lidard, W. Lau, and J. Simpson, 2009: A multi-scale modeling system: Developments, applications, and critical issues. *Bull. Amer. Meteor. Soc.,* **90***,* 515-534.

Thayer-Calder, K., and D. A. Randall, 2009: The Role of Convective Moistening in the Formation and Progression of the MJO. *J. Climate*, **66**, 3297-3312.

Tomita, H., H. Miura, S. Iga, T. Nasuno, and M. Satoh, 2005: A global cloud-resolving simulation: Preliminary results from an aqua planet experiment, *Geophys. Res. Lett.*, **32**, L08805, doi:10.1029/2005GL022459.

Tung, W.-W., and M. Yanai, 2002 a: Convective Momentum Transport Observed during the TOGA COARE IOP. Part I: General Features. *J. Atmos. Sci.*, **59**, 1857-1871. doi: http://dx.doi.org/10.1175/1520-0469(2002)059<1857:CMTODT>2.0.CO;2

Tung, W.-W., and M. Yanai, 2002 b: Convective Momentum Transport Observed during the TOGA COARE IOP. Part II: Case Studies. *J. Atmos. Sci.*, **59**, 2535-2549. doi: http://dx.doi.org/10.1175/1520-0469(2002)059<2535:CMTODT>2.0.CO;2

Wheeler, M., and G. N. Kiladis, 1999: Convectively Coupled Equatorial Waves: Analysis of Clouds and Temperature in the Wavenumber-Frequency Domain. *J. Atmos. Sci.*, **56**, 374-399. doi: http://dx.doi.org/10.1175/1520-0469(1999)056<0374:CCEWAO>2.0.CO;2

Wu, X., and M. Yanai, 1994: Effects of Vertical Wind Shear on the Cumulus Transport of Momentum: Observations and Parameterization. *J. Atmos. Sci.*, **51**, 1640-1660. doi: http://dx.doi.org/10.1175/1520-0469(1994)051<1640:EOVWSO>2.0.CO;2

Wyant, M. C., M. Khairoutdinov, and C. S. Bretherton, 2006: Climate sensitivity and cloud response of a GCM with a superparameterization. *Geophys. Res. Lett.*, **33**, L06714, doi:

10.1029/2005GL025464

Wyant, M.C, C.S. Bretherton, P. N. Blossey, and M. Khairoutdinov, 2012: Fast Cloud Adjustment to Increasing CO2 in a Superparameterized Climate Model. *J. Adv. Model Earth Syst.*, **4**, M05001, doi:10.1029/2011MS000092.

Xu, K.-M., and A. Cheng, 2013 a: Evaluating low-cloud simulation with an upgraded multiscale modeling framework model. Part I: Sensitivity to spatial resolution and climatology. *J. Climate,* **26**, 5717-5740.

Xu, K.-M., and A. Cheng, 2013 b: Evaluating low-cloud simulation with an upgraded multiscale modeling framework model. Part II: Seasonal variations over the Eastern Pacific. *J. Climate,* **26**, 5741-5760.

Yamaguchi, T., D. A. Randall, and M. Khairoutdinov, 2011: Cloud Modeling Tests of the ULTIMATE-MACHO Scalar Advection Scheme. *Mon. Wea. Rev.* , **139**, 3248-3264.

Yanai, M., and C. Li, 1994: Mechanism of Heating and the Boundary Layer over the Tibetan Plateau. *Mon. Wea. Rev.*, **122**, 305-323. doi: http://dx.doi.org/10.1175/1520-0493(1994)122<0305:MOHATB>2.0.CO;2

Figure Captions

Fig. 1: In conventional GCMs, the global circulation is explicitly simulated. Parameterized processes include cloud-scale and mesoscale dynamics, and also radiative transfer, microphysics, and turbulence.

Fig. 2: When a CRM is used as a super-parameterization in a GCM, the cloud and mesoscale dynamics are explicitly simulated, but radiation,microphysics, and turbulence must still be parameterized on the CRM's grid. Compare with Fig. 1.

Fig. 3: Schematic illustrating the coupling of the GCM and the CRM, in the SP-CAM.

Fig. 4: Time-longitude structure of warm season diurnal convective activity in the lee of the Rocky Mountains between 35˚N and 45˚N, and plotted for longitudes between 250˚ and 280˚ E. Each panel shows the longwave cloud forcing, bandpass filtered to include periods between 12 and 48 hours, plotted over a period of 30 days.The left panel shows SP-CAM5, the center panel shows observations, and the right panel shows CAM5. Based on Kooperman et al. (2013).

Fig. 5: (a) The observed climatological precipitation rate for July. (b) The simulated climatological precipitation rate for the SP-CAM. (c) The difference between the SP-CAM results and the observations. (d) The simulated climatological precipitation rate for the coupled ocean-atmosphere model, SP-CCSM. (e) The difference between the SP-CESM results and the observations. (f) The difference between the SP-CESM results and the SP-CAM results. Adapted from Stan et al. (2010). For precipitation rate maps, the contour interval is 2 mm day^{-1}, and values larger than 4 mm day^{-1} are shaded. For the difference maps, the contour interval is again 2 mm day^{-1}, values larger than 2 mm day^{-1} have dark shading, and values smaller than -2 mm day^{-1} have light shading.

Fig. 6: Composite profiles of relative humidity binned by daily average rain rate in the region from 15ºS to 15ºN, and from 50ºE to the Date Line . The contour interval is 10%, and the 70% contour is heavy. From Thayer-Calder and Randall (2009).

Figure 7: Correlations of the lagged 850 zonal wind with equatorial rainfall at 90°E for: (a) observations (ERA-Interim and GPCP), (b) SPCAM with prescribed seasonally varying sea surface temperatures, and (c) SPCAM-SOM. All fields are filtered to pass only MJO time scales, and merdionally averaged near the Equator. The horizontal axis is longitude relative to the Greenwich meridian, and the vertical axis is lag in days relative to the time of maximum precipitation at 90°E. The 5 m s^{-1} phase speed is shown with a thick black line. The contour interval is 0.1, with positive contours solid, negative contours dashed, and the zero contour omitted. Dark (light) gray shading denotes correlations greater than 0.2 (less than –0.2). Adapted from Benedict and Randall (2011).

Figure 8: May-October MJO precipitation variance as a function of longitude for GPCP, SP-CCSM3, SP-CAM3, and CCSM3. Precipitation is filtered to retain 20-100 day variability and eastward-propagating wave numbers 1-6. Data are averaged from 5-25ºN.

Figure 9: Signal-to-noise ratio of equatorially-antisymmetric component of OLR in observations, SPCCSM3, SPCAM3, and CCSM3. The dispersion relation for typical equivalent depths are indicated by solid lines. The "observed" feature near zonal wave number 15 and frequency 0.12 day^{-1} is spurious, and arises from aliasing of the satellite data. Here "MRG" refers to mixed Rossby-gravity waves, and "EIG" refers to eastward inertial-gravity waves.

Figure 10: JJA lag-correlation of 20-100 day filtered precipitation with itself in GPCP, SP-CCSM, SP-CAM, and CCSM. The "3" on the end of SP-CCSM3 and SP-CAM3 and CCSM3 refers to version 3 of the CAM, which was used as the GCM in these simulations. The base point time series is the filtered precipitation averaged over 10ºS-5ºN, 80º-100ºE. The contour interval is 0.2, with positive (negative) values shown with solid (dashed) lines.

Figure 11: Longitude-height cross section of the specific humidity anomaly in African Easterly Waves as observed (left), as simulated by the SP-CCSM (middle) and as simulated by CCSM3 (right). The latitude is 10ºN. Units are g kg^{-1}. The heavy contour is zero, dashed contours are negative (lightly shaded) and solid contours are positive (darkly shaded). The contour interval for the SP-CCSM results is 0.05 g kg^{-1}, while the contour interval for the observations and for CCSM is 0.02 g kg^{-1}. The small plots at the top of each panel show anomalies of the outgoing longwave radiation, in W m^{-2}. The anomalies of both water vapor and outgoing longwave radiation are relative to seasonal means. Based on the work of McCrary (2012).

Fig. 12: Plots of simulated years per wall-clock day versus the number of processors used, for the conventional CAM (dots) and the SP-CAM (squares). The GCM grid spacing is 2.5º of longitude by 2º of latitude for both models. Note that the axes are logarithmically scaled. The figure shows that, with this resolution, the SP-CAM can efficiently use thousands of processors, while the CAM is limited to hundreds. The timing tests were performed on Hopper, a Cray XE6 at the National Energy Research Scientific Computer Center (NERSC), by Mark Branson of Colorado State University.

Figure 13: In this Venn diagram, the circle on the left represents process models, and the circle on the right represents global atmospheric models. Until recently, these two classes of models did not overlap. Today, as shown in the figure, there is some intersection in the form of GCRMs and MMFs. This figure first appeared in Randall (2013).